Pergamon

Geochimica et Cosmochimica Acta, Vol. 65, No. 10, pp. 1665–1678, 2001

0016-7037/01 $20.00 + .00

PII S0016-7037(00)00625-6

Transition elements in water-bearing silicate glasses/melts. Part I. A high-resolution and anharmonic analysis of Ni coordination environments in crystals, glasses, and melts

FRANÇOIS FARGES,[1,2,*] GORDON E. BROWN, JR.,[2,3] PIERRE-EMMANUEL PETIT,[4] and MANUEL MUNOZ[1]

[1]Laboratoire des géomatériaux, Université de Marne-la-Vallée, and Ecole Nationale Supérieure des Mines de Paris 77454 Marne la Vallée Cedex, France
[2]Department of Geological and Environmental Sciences, Stanford University, Stanford, CA 94305-2115, USA
[3]Stanford Synchrotron Radiation Laboratory, SLAC, P.O. Box 4349, Stanford University, Stanford, CA 94309, USA
[4]European Synchrotron Radiation Facility BP 220, 38043 Grenoble Cedex, France

(*Received December* 11, 1999; *accepted in revised form November* 28, 2000)

Abstract—The local structural environment around Ni(II) in a series of crystalline model compounds and K-Ni-, Na-Ni-, and Ca-Ni-silicate glasses and melts has been evaluated by using high-resolution Ni K-edge XANES spectroscopy and anharmonic EXAFS data analysis. The glasses show NBO/T contents ranging from 0 (albitic composition) to 1 (alkali-disilicate composition) and Ni contents ranging from 40 ppm to 2 wt.%.

The pre-edge feature for model compounds vary not only in normalized height as a function of Ni-coordination but also in position (by ~0.5 eV) as confirmed by ab initio XANES calculations. In addition, the pre-edge position is indirectly correlated with the average Ni-O distance. By using these correlations, Ni is predicted to be 4-coordinated, on average, in the potassic glasses, ~5-coordinated in the sodic glasses, and >5-coordinated in the calcic glasses. The EXAFS-derived distances and coordination numbers are consistent with these conclusions, with the average Ni-O distances ranging between 1.96 and 2.03(2) Å. In contrast, NiO_4 units are dominant in the melts examined (Na-disilicate composition with 4000 ppm of Ni).

Variation in NBO/T or in Ni concentration does not affect the local environment of Ni in these silicate glasses whereas the type of network modifier present in the glass (K vs. Na vs. Ca + Mg) does. This finding explains the overall good agreement between this study and a previous XAFS study on silicate glasses with higher Ni concentrations and less polymerization (Galoisy and Calas, 1993a). In Part 2 of this series, these new correlations between Ni K-pre-edge features and Ni coordination number are used to characterize Ni structural environments in sodium trisilicate and albitic glasses containing 2000 ppm of Ni and exposed to pressures up to 5 kbars with 0 to 8 wt.% water. These hydrated glasses show major changes in their crystal field spectra, which correspond to major changes in the local coordination environment of Ni as revealed by XAFS spectroscopy. *Copyright © 2001 Elsevier Science Ltd*

1. INTRODUCTION

Nickel is an important trace cation in silicate minerals and melts and is known to partition strongly from silicate melts into metallic or oxide crystals (Takahashi, 1978; Mysen et al., 1982; Colson et al., 1988; Seifert et al., 1988; Burns, 1993; Malavergne et al., 1997; Taura et al., 1998). In addition, the crystal-chemistry of (divalent) nickel was extensively studied in light of the thermodynamic and rheological properties of silicate melts, especially during basalt production and migration (Kinzler, 1990; Dingwell et al., 1994; Holzheid et al., 1996; Courtial et al., 1997; Ertel et al., 1997). A fundamental understanding of the partitioning behavior, including possible changes in the structural environment of Ni(II) in the melt as a function of melt composition, temperature, pressure, pH_2O, and other variables is required for understanding processes such as differentiation in the Earth's mantle and core, which are believed to be major Ni reservoirs.

The coordination environment of Ni(II) in silicate melts has long been inferred from ambient temperature/pressure crystal-field spectroscopy on Ni-bearing glasses. In sodic silicate glasses, Ni is believed to occur in a mixture of 4-, and 6-coordinated environments (Calas and Petiau, 1983; Burns, 1993) or in distorted 6-coordinated environments (Keppler, 1992). Another interpretation of crystal-field spectra for sodic silicate glasses (Galoisy and Calas, 1993a) concluded that Ni(II) is dominantly 5-coordinated (as trigonal bipyramids), with some variable amount of tetrahedrally coordinated Ni(II). Parallel X-ray absorption fine structure (XAFS) spectroscopy studies of Ni (≈2000 ppm) in silicate glasses and melts (Galoisy and Calas, 1993a; Farges et al., 1994; Farges and Brown, 1996) confirmed the presence of 5-coordinated Ni(II) in sodic silicate glasses, a result that is also consistent with a neutron scattering study of Ni-bearing sodium silicate glass (Gaskell et al., 1992). This model has recently been questioned by Nowak and Keppler (1998) who concluded that near infra-red spectra of albitic glasses containing ≈4000 ppm of Ni are inconsistent with the presence of 5-coordinated Ni environments. However, the glasses investigated in the earlier ultraviolet/vis, XAFS, neutron scattering, and infrared studies had somewhat different bulk compositions, including different Ni concentrations, which may explain the different interpretations.

Here, we present the results of a high-resolution XAFS spectroscopy study, including theoretical modeling of the pre-edge, XANES and EXAFS spectral regions, of Ni(II) in several Na-Ni-, K-Ni-, and Ca-Ni-silicate glasses with various NBO/T ratios (ranging from 0 to 1) and Ni-contents (ranging from 40 ppm to 2 wt.%). The coordination environment of Ni(II) was analyzed by using empirical correlations between Ni K-pre-

* Author to whom correspondence should be addressed (farges@univ-mlv.fr).

Table 1. Synthesis conditions and electron microprobe analysis for selected glasses.

Glass	Temp. (°C)	Duration (h)	NiO	SiO_2	Al_2O_3	Na_2O	K_2O	CaO	MgO	Σ
KS3 0.4	1100	4	0.3	69.3			29.4			99.0
$Na_2NiSi_3O_8$	1550	1	22.7	56.9		20.3				99.9
NS2 2	1200	4	2.0	65.5		32.4				99.9
NS3 2	1200	4	1.9	72.6		25.3				99.8
ALB 0.4	1550	4	0.3	68.9	19.1	12.0				100.3
Ni : $CaMgSi_2O_6$	1550	12	1.4	55.6				25.5	17.4	99.9
Average error	20	0.1	0.2	0.8	0.5	1.5	1.0	0.3	0.3	

edge intensity and energy position in crystalline model compounds containing Ni(II) in different coordination environments. Ab initio multiple-scattering calculations of the pre-edge and XANES spectra are also presented and are compared with the experimental spectra. The Ni(II) coordination environments in these glasses were also evaluated by using average Ni-O distances and coordination numbers derived from an anharmonic analysis of EXAFS data. In addition, we report quantitative evaluations of the effects of disorder, based on ab initio calculations of the XAFS spectra (pre-edge, XANES and EXAFS) and the influence of multiple scattering around Ni on the experimental spectra. The conclusions from this study are similar to those reported earlier by Galoisy and Calas (1993a, b) for more Ni-rich and less polymerized silicate glass compositions, and they establish experimental and theoretical protocols for collecting and interpreting XAFS spectra of Ni(II) in water-bearing Na-Ni-silicate glasses presented in Part 2 (Farges et al., 2000).

2. ANALYTICAL METHODS

2.1. Model Compounds

$NiCr_2O_4$ and Rb- and $Cs_2NiSi_5O_{12}$ leucites were used as models for 4-coordinated Ni(II), designated by $^{[4]}$Ni (Manceau and Calas, 1986; Bell and Henderson, 1996). $K^{[5]}NiPO_4$ was used as a model for 5-coordinated Ni(II) (Lyutin et al., 1973). Model compounds containing 6-coordinated Ni(II) were $^{[6]}$NiO (green: Bobrovskii et al., 1973), $Ca^{[6]}NiSi_2O_6$ (Ghose et al., 1987), α-$^{[6]}Ni_2SiO_4$ (olivine polymorph; Lager and Meagher, 1978), nepouite, $^{[6]}Ni_2Si_2O_5(OH)_4$ (Brindley and Wan, 1975), α-$^{[6]}Ni(OH)_2$ (Greaves and Thomas, 1986), as well as $^{[6]}NiTiO_3$ and $^{[6]}NiAl_2O_4$. To test our methods, we also studied several samples that contain Ni(II) at more dilute levels, including Ni-bearing-olivine and diopside (Ni occupying 10 mol.% of the octahedral sites) and Ni sputtered on γ-Al_2O_3 (Ni : Al_2O_3).

2.2. Silicate Glasses

The glass compositions studied were prepared by mixing appropriate amounts of dehydrated, reagent grade oxides (SiO_2, Al_2O_3, NiO), and dried carbonates (Na_2CO_3, K_2CO_3, $CaCO_3$) in an agate mortar, decarbonating (by heating slowly from 20–800°C over 12 h), and melting in a Pt crucible. The melts were quenched and the resulting glasses were reground then remelted and quenched to enhance homogeneity. Some Ni (10–20 atom.%) was lost to the Pt-crucible during melting. Glass compositions determined by electron microprobe analysis are listed in Table 1 and are within 95% of their nominal compositions. KS2 and KS3 stand for potassium di- and trisilicate compositions (nominally $K_2Si_2O_5$ and $K_2Si_3O_7$). Similarly, NS2, NS3, and NS4 are the designations for sodium di-, tri-, and tetrasilicate compositions ($Na_2Si_2O_5$, $Na_2Si_3O_7$, and $Na_2Si_4O_9$). ALB represents an albitic composition ($NaAlSi_3O_8$). The designation "NS2 2" represents a sodium disilicate glass with 2 wt.% Ni. Similarly, "ALB 0.4" is the designation for an albitic glass with 4000 ppm Ni.

2.3. XAFS Data Collection

Ni K-pre-edge, XANES, and EXAFS spectra for model compounds and glasses were collected at the Stanford Synchrotron Radiation Laboratory (Palo Alto, CA, USA) on wiggler beam line IV-1 at the Ni K-edge (8.33 keV). The storage ring operating conditions were 3 GeV electron energy and 30 to 100 mA electron current. A Si(220) double-crystal monochromator was used for these experiments (energy resolution [FWHM] of ~1.5 eV at the Ni K-edge for a beam height of ~1 mm). To remove the high-energy harmonics from the incident X-ray beam, the monochromator was detuned so that the intensity of the incoming beam was reduced by 25%. XAFS data for most model compounds and $Na_2NiSi_3O_8$ glass were collected in transmission mode because of their high Ni-contents. The optimum thicknesses of samples for transmission experiments were calculated by using the computer code "absorbance 2.1" (written by F. Farges) to result in an absorbance (μ) and an edge jump ($\Delta\mu/\mu$) close to 1 at 8.5 keV (typical thicknesses are 5–30 μm depending on Ni concentration). The appropriate amounts of powdered model compounds (size fraction below 50 μm) were mixed with boron nitride to reach a dilution level corresponding to the calculated theoretical thickness. Each mixture was compacted in a Teflon sample holder of 1 mm thickness, with Kapton windows (20 μm thickness). A Cu-foil was used to provide an accurate and absolute energy calibration of the monochromator (Pettifer and Hermes, 1985).

For the model compounds and glasses with more dilute Ni concentrations (such as Ni : Al_2O_3 and the albitic glasses for which self-absorption effects are negligible), XAFS spectra were collected in the fluorescence mode. Powdered samples were loaded into 2-mm-thick Teflon sample holders. The incident- and transmitted-beam intensities were monitored with ionization chambers by using N_2 as the absorbing gas. The fluorescence yield was measured as a function of X-ray energy by using a Stern–Heald-type detector (Lytle et al., 1984) with Xe in the fluorescence detector ion chamber. A CoO filter (3 μ absorbance) and Ag-Soller slits were used to minimize unwanted elastic scattering and filter fluorescence, respectively. In order to monitor energy calibration during data collection, a third ionization chamber (filled with Ar) was used to collect XAFS spectra on crystalline NiO in transmission mode simultaneously with the collection of fluorescence XAFS spectra of the models compounds and glasses. The reproducibility level of the high-resolution XANES spectra for all samples was 0.05 eV, based on the pre-edge position for NiO, measured at 8331.25 eV compared to metallic Ni.

XANES spectra were collected from 130 eV below to 220 eV above the Ni K-edge (8200–8550 eV), with 0.5 eV steps, to allow a proper normalization of these spectra in height. Energy steps of 0.05 eV were used for the pre-edge region (8326–8334 eV). We used a reduced height for the horizontal slits (0.3 mm) to collect the XANES spectra under relatively high-resolution conditions (see below). This protocol results in enhanced resolution of pre-edge and XANES features, but it does not affect the EXAFS region of the spectrum where features are not as well defined (Fig. 1). The Ni pre-edge spectra for most model compounds and glasses were collected twice within a 1-yr interval to check for reproducibility; no differences were observed between duplicate spectra.

In contrast, we used low-resolution conditions (2 mm vertical slits after the monochromator) to achieve the higher flux needed for collecting high-quality EXAFS spectra up to 9200 keV. Step sizes varied from a minimum of 2 eV in the low energy region to a maximum of 5

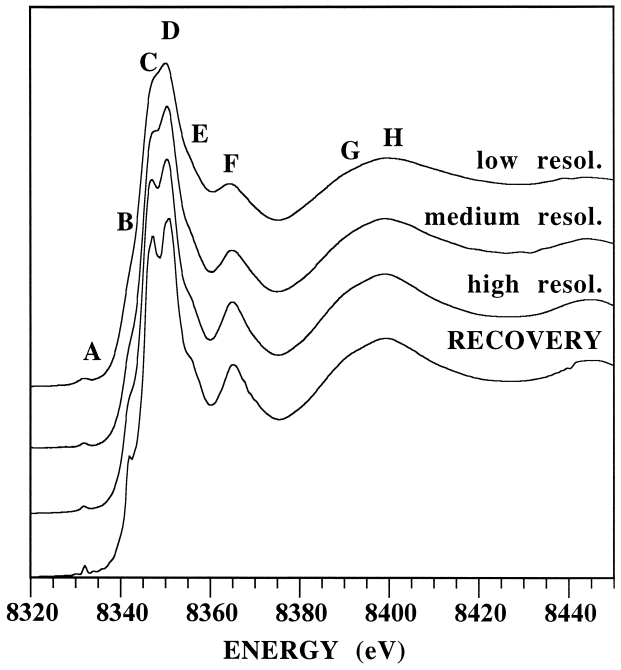

Fig. 1. Ni K-edge XANES spectra collected for nepouite ($^{[6]}Ni_2Si_2O5_5(OH)_4$) under low-, medium-, and high-resolution conditions, respectively, at LURE on the EXAFS2 spectrometer by using Si(311)-monochromator crystals; at SSRL on BL 4-3 using Si(220)-monochromator crystals and 2-mm vertical aperture slits; and at ESRF on ID26 using Si(220)-monochromator crystals and 0.3 vertical aperture slits. The bottom curve is the spectrum calculated from the top spectrum (LURE), using the deconvolution RECOVERY package, which removed the experimental broadening of the high-resolution spectrum using Shannon's information theory (Kosarev, 1990).

eV at the highest energies of the scan (equivalent to constant *k*-steps of 0.05/Å). For glasses with dilute Ni concentrations, 4 to 16 EXAFS scans were averaged together to increase the signal-to-noise ratio.

In situ, high-temperature XANES spectra were collected at the ESRF (Grenoble, France) on the new undulator beamline ID26 designed for collecting XAFS spectra on ultradilute samples (Gauthier et al., 1999; Solé et al., 1999). The storage ring operating conditions were 6 GeV electron energy and 140 to 200 mA electron current. The first harmonic of a 35-mm period undulator was used, as well as a Si(220) double-crystal monochromator. Harmonics rejection and focusing were performed by using a flat mirror coated with amorphous Si and a curved bimorph SiO_2 mirror. The second mirror focus the beam in the horizontal plane, and the spot size on the sample was typically 0.3 × 1.5 mm. XANES spectra were collected at the Ni K-edge by using a fluorescence-mode furnace (see Farges et al., 1994 for details on data collection and temperature control). Fast, highly linear, and low-noise Pin diodes detectors were used to monitor the beam intensity (using a Ti fluorescence foil) and to detect the fluorescence signal (using a CoO filter of 6 μ absorbance to minimize the elastic scattering).

2.3. XAFS Data Analysis

2.2.1. Pre-edge and XANES spectra

Pre-edge and XANES spectra were reduced by using a protocol described in Farges et al. (1996a). In order to test the energy resolution of our XANES experiments, we have collected Ni K-edge XANES spectra for the nepouite model compound by using synchrotron radiation arising from storage rings of different generation (first, second, and third generations, using the spectrometers "EXAFS2," "4-3," and "ID26" at the LURE, SSRL, and ESRF facilities, respectively; Fig. 1). Each of these spectra were collected under the highest resolution possible locally. To compare these spectra, the spectrum collected at LURE was deconvoluted by using the RECOVERY computer code (Kosarev, 1990), which removes the spectral distortion inherent to any experimental measurement. This method is based on the Maximum Likelihood principle, which allows the maximum value of resolution improvement to be achieved according to Shannon's information theory. We chose a point spread function (PSF) as a Gaussian function of 1.6 eV, assuming the estimated core-hole width of Ni (1.2 eV) (Brown, 1980) and an experimental convolution of 0.4 eV. Analysis of RECOVERY data processing suggests that the high-resolution XANES spectrum of nepouite collected at ESRF (third generation source) is close to the broadening-free spectrum. On this absolute resolution scale, the "high-resolution" XANES spectra from beamline 4-3 at SSRL (second generation) were in fact collected under a "medium" resolution. A major application of this new strategy is the analysis of disorder effects in materials. XANES spectra for well locally structured materials will benefit highly from third generation sources (dramatic improvement in resolution, as for nepouite), whereas disordered materials won't benefit as much (as we tested this on the glasses and melts of this study). Also, we found that the deconvoluted pre-edge spectrum (Fig. 1) consists of one main feature, in agreement with theory (see below). Finally, a deep improvement in the robustness of theoretical XANES calculations can be performed on such deconvoluted spectra, as new features are revealed.

Thus, XANES spectra were modeled by using the ab initio code FEFF (Version 8.2; a β-release; Rehr et al., 1992; Ankudinov et al., 1998), which is based on full multiple scattering (FMS) theory and provides better convergence in this energy region. We optimized the choice of parameters in the FEFF8 calculations to result in a close match between the calculated and experimental spectra for model compounds, as outlined previously elsewhere (Farges et al., 1996a). A self-consistent field (SCF) multiple-scattering (MS) procedure was used to better model charge transfer between atoms during the photoelectric process in a cluster consisting of ~30 to 50 atoms (up to 4 Å around the central atom) in $NiCr_2O_4$, $KNiPO_4$, and nepouite (card "SCF 4.0") (13 iterations were required before reaching convergence and Hedin–Lunqvist potentials were used). Then, the XANES spectra were calculated assuming the full-multiple scattering formalism (including quadrupolar elements): card "FMS 2.5 0").

2.4.2. EXAFS spectra

EXAFS spectra were analyzed in accordance with the International XAFS Standards and Criteria established by the International XAFS Society using the XAFS package (version 2.5b; Winterer, 1996). XAFS spectra were normalized in absorbance by using a Victoreen and a cubic spline function (with ≈10 external double knots, which provided an excellent background subtraction). E_0 was determined as the inflection point of an error function fit to the edge jump (≈8338 ± 1 eV). The normalized EXAFS oscillations were k^3-weighted (range 1–13/Å) and Fourier transformed (FT) by using a Kaiser–Bessel filter (with a τ values of 4). The normalized, k^3-weighted EXAFS oscillations were modeled by using a theoretical EXAFS spectrum calculated with FEFF8 for a NiO_4Si_4 cluster (as in $Cs_2NiSi_5O_{12}$; Bell and Henderson, 1996). Disorder effects were modeled by using the cumulant expansions theory (Crozier et al., 1988).

Based on previous low-temperature EXAFS measurements (Galoisy and Calas, 1993a), the influence of thermal disorder at 20°C is negligible as compared to structural disorder. At high temperatures, the use of cumulant expansions has been shown to be acceptable in accounting for anharmonicity effects in Ni K-edge EXAFS spectra at temperatures up to 1150°C (Farges et al., 1994).

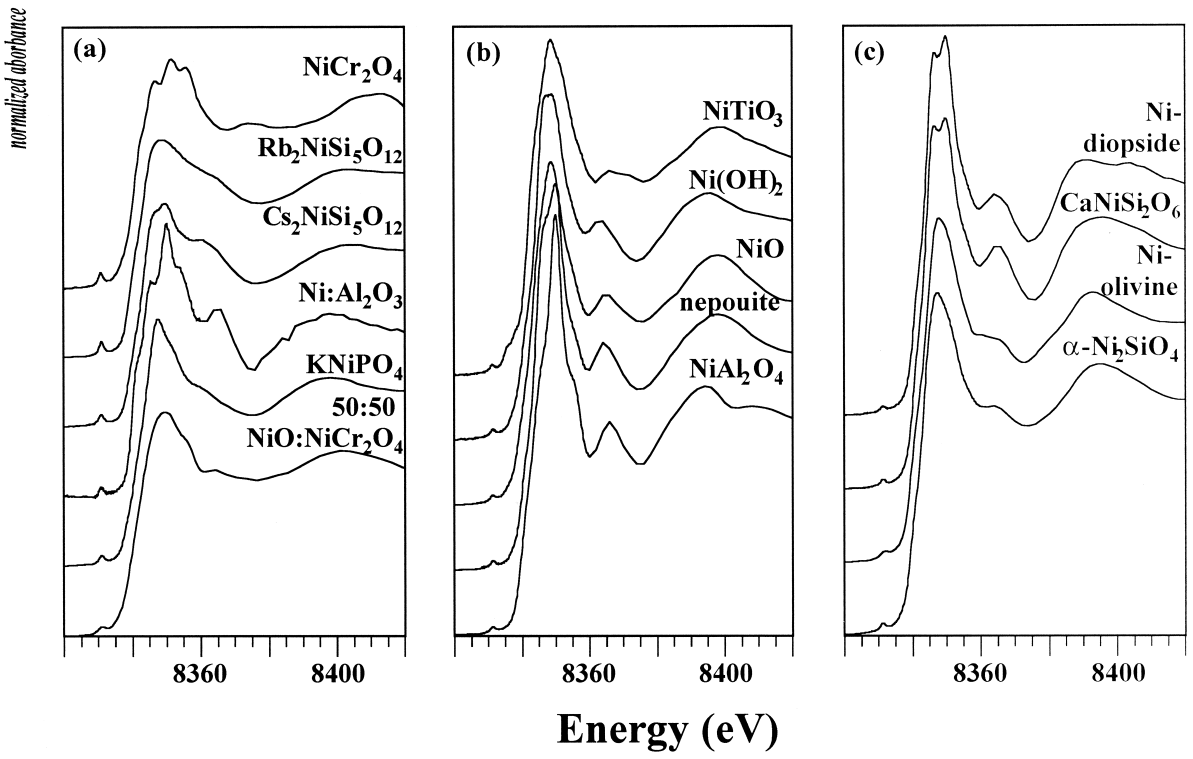

Fig. 2. High-resolution Ni K-edge XANES spectra for model compounds in which Ni(II) is 4, and 5-coordinated (a, left), or 6-coordinated (b, middle; and c, right).

3. RESULTS

3.1. Pre-edge Features and XANES Spectra

3.1.1. Model compounds

Pre-edge features (feature A on Fig. 1) are most likely due to the transition of a 1s electron of Ni from its core atomic state to a final unoccupied state (a relaxed excited state due to the presence of a core hole screened by the other electrons of Ni). In addition, within the dipole approximation (ground and relaxed states have the same parity), a transition to the final state (here a third state) is not Laporte forbidden as long as the final state has some metal 4p (Westre et al., 1997) and/or ligand 2p character from the oxygen ligands (Kuzmin et al., 1997). Ab initio simulations of the pre-edges of Ni have not been successful until recently (e.g., Garcia et al., 1995; Kuzmin et al., 1997) because of the amount of p-d mixing, which makes the theoretical simulations more challenging. However, a multiplet analysis of Ni pre-edges would be required for a more complete understanding of the origin of the Ni K-pre-edge feature.

Figure 2 shows the normalized XANES spectra for Ni(II)-bearing model compounds for which the position and height of the pre-edge feature have been evaluated. In addition to the well-established changes in pre-edge height as a function of Ni-coordination (see Calas and Petiau, 1985; Manceau and Calas, 1985; Galoisy and Calas, 1993a), the normalized pre-edges for $^{[4]}$Ni(II), $^{[5]}$Ni(II), and $^{[6]}$Ni(II) show different energy positions (Fig. 3a). This is due to the fact that the third orbitals are nearly filled and only the less energetically favorable orbitals are able to receive a core 1s electron. Because the Fermi level is located between the energetically favorable orbitals (all occupied) and the partially empty and energetically unfavorable orbitals (see also Heumann et al., 1997), the 1s-3d transition will occur at different energies, depending on crystal field splitting.

The plot of pre-edge absolute position versus normalized intensity (Fig. 3b) shows distinct domains for $^{[4]}$Ni, $^{[5]}$Ni, and $^{[6]}$Ni. The average pre-edge positions for $^{[4]}$Ni and $^{[6]}$Ni are separated by $\sim$0.5 eV. Figure 3b also suggests that the use of the pre-edge height alone gives less robust information on Ni coordination number. Indeed, a more centrosymmetric site with a lower Ni-coordination (such as in $K^{[5]}NiPO_4$) has a pre-edge height similar to that of a less centrosymmetric, but more highly coordinated Ni-environment (such as $Ca^{[6]}NiSi_2O_6$). However, we can clearly distinguish between distorted NiO_6 and (regular or distorted) NiO_5 environments based on a combination of pre-edge position and normalized height.

The position and height of pre-edge features for Ni-bearing olivine and diopside (Table 2) are similar to those measured for α-Ni_2SiO_4, $CaNiSi_2O_6$, and the other compounds examined here containing regular or distorted 6-coordinated Ni(II). Finally, the pre-edge for Ni-sputtered on γ-Al_2O_3 (Ni : Al_2O_3) is consistent with the presence of $^{[4]}$Ni, in agreement with its optical absorption spectrum (Galoisy and Calas, 1993a).

Theoretical multiple-scattering calculations of the Ni K-edge XANES spectra using FEFF8 (Fig. 4) confirmed that the edge crest (feature C) and the first EXAFS oscillation (feature E) are shifted toward lower energy with increasing Ni(II)-coordination. Also, our calculations show that feature D results from

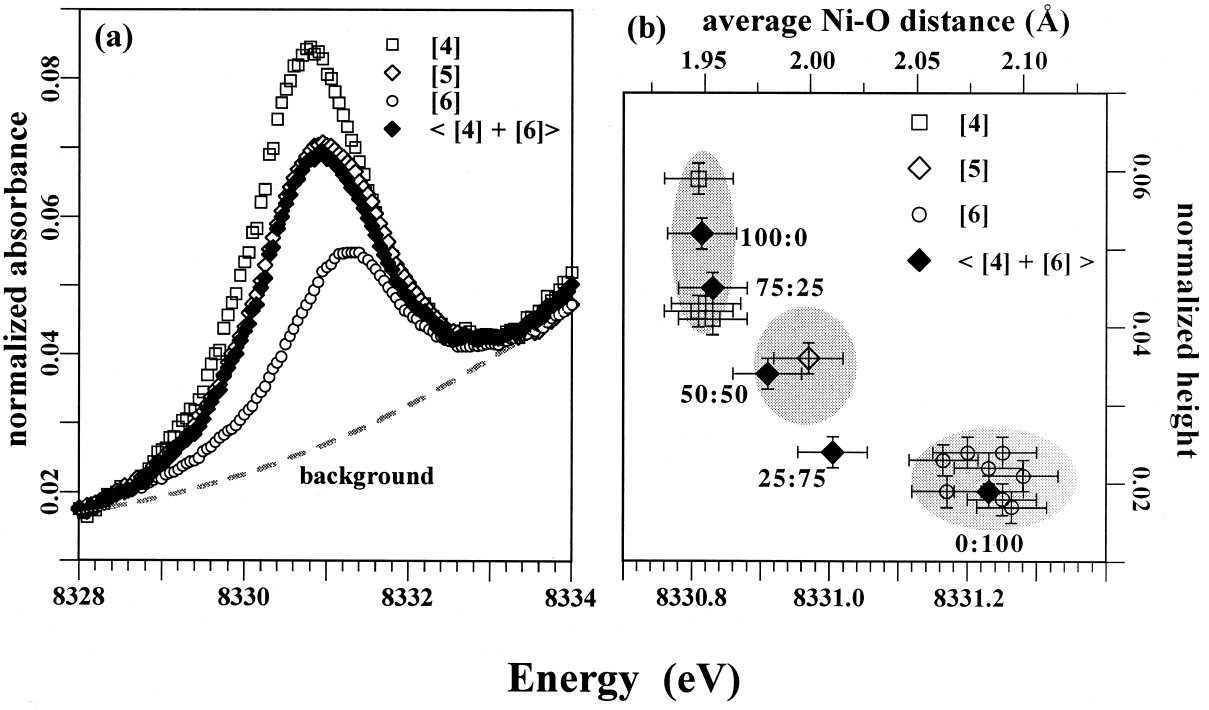

Fig. 3. (a, left) Comparison of pre-edge features for 4, 5-, and 6-coordinated Ni(II) (open squares, diamonds and circles, respectively) as compared to that for a 50 : 50 mixture of 4-, and 6-coordinated Ni(II) (black diamonds); (b, right) Plot of the pre-edge information (energy position, bottom axis vs. normalized height, vertical axis) for the model compounds of this study and the mixtures between 4- and 6-coordinated Ni(II). Also shown on the top x-axis is the corresponding average Ni-O distance measured in these model compounds by using X-ray or neutron scattering methods.

multiple-scattering effects, which are enhanced in highly centrosymmetric polyhedra like a regular octahedron. Finally, the pre-edge (feature A) varies in absolute position and relative height with varying Ni(II)-coordination as observed experimentally: when Ni(II) is tetrahedrally coordinated, the normalized pre-edge is shifted toward lower energies by ~0.55 eV as compared to 6-coordinated Ni(II). Also, the calculated pre-edge height of $^{[4]}$Ni is twice that of $^{[5]}$Ni(II), in excellent agreement with our experimental results (0.062 and 0.036; Table 2). Thanks to the use of FEFF8.2, we were able to calculate well-resolved pre-edges for 6-coordinated Ni(II), as these features are related mostly to quadrupolar transitions (Heumann et al., 1997). Finally, feature B (often partially hidden by the edge jump) is probably related to a 1s → 4s transition as for Fe(II) (Waychunas et al., 1983) which are enhanced for centrosymmetric environments. However, more detailed studies are re-

Table 2. Ni pre K-edge information for selected Ni(II) model compounds.

	Pre-edge information		
Model compound	Normalized height	Absolute position (eV)	Half-width (eV)
$^{[4]}NiCr_2O_4$	0.062	8330.81	1.48
$Cs_2{}^{[4]}NiSi_5O_{12}$	0.042	8330.80	1.51
$^{[4]}Ni : Al_2O_3$	0.041	8330.83	1.50
$50 : 50\ ^{[4]}Ni - {}^{[6]}Ni$[a]	0.042	8331.00	1.58
$K^{[5]}NiPO_4$	0.036	8330.97	1.61
$^{[6]}Ni_3Si_2O_5(OH)_4$	0.021	8331.28	1.39
$^{[6]}NiO$	0.018	8331.25	1.25
α-$^{[6]}Ni(OH)_2$	0.022	8331.23	1.30
α-$^{[6]}Ni_2SiO_4$	0.023	8331.17	1.43
$Ca^{[6]}NiSi_2O_6$	0.019	8331.17	1.34
$^{[6]}NiTiO_3$	0.024	8331.25	1.46
α-$(Mg_{0.9}{}^{[6]}Ni_{0.1})_2SiO_4$	0.024	8331.20	1.42
$Ca(Mg_{0.9}{}^{[6]}Ni_{0.1})Si_2O_6$	0.017	8331.26	1.46
Average error	0.002	0.05	0.05

[a] as $NiCr_2O_4$ for $^{[4]}$Ni and NiO for $^{[6]}$Ni.

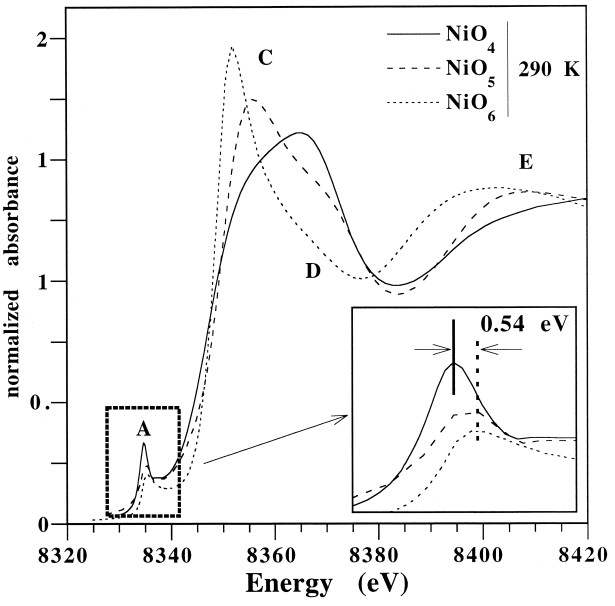

Fig. 4. Calculated XANES spectra (using FEFF 8.2, including quadrupolar transitions) for 4-, 5-, and 6-coordinated Ni(II), showing variation in the pre-edge feature (A), the edge crest (feature C), and the first EXAFS oscillation (E). Atomic clusters for these spectra were taken from the local structure around Ni in $NiCr_2O_4$, $KNIPO_4$, and nepouite, respectively. Inset: zoom of the pre-edge feature (A), showing variation in pre-edge absolute position and normalized height with Ni(II)-coordination, consistent with the experiment.

quired to ascertain the origin of this feature, as it can be due to metallic Ni or a transition involving second neighbors nickel orbitals.

3.1.2. Mixtures of coordinations

The pre-edge information for an experimental analysis of six different mixtures of $^{[4]}$Ni(II) and $^{[6]}$Ni(II) (in the form of X $^{[4]}NiCr_2O_4$ + (1 − X) $^{[6]}$NiO) is shown in Figure 3b. The pre-edge position and height vary slightly hyperbolically as a function of the average Ni-coordination (Fig. 3b). However, within uncertainties, this variation is quasi-linear. In particular, the pre-edge information for the 50 : 50 mixture of $^{[4]}$Ni and $^{[6]}$Ni is located roughly half-way between those for $NiCr_2O_4$ and NiO. Therefore, it is not possible here to distinguish clearly between a sample containing 100% $^{[5]}$Ni and one containing 50% $^{[4]}$Ni + 50% $^{[6]}$Ni. By using pre-edge information, we can only determine the average Ni-coordination, even under high-resolution conditions. However, because of the quasi-linear variation of the pre-edge position as a function of Ni coordination, the pre-edge position is linearly correlated with the average Ni-O distance (see Fig. 3b, top scale, using crystal structure information for the model compounds). This correlation between the pre-edge position an the average Ni-O distance is indirect: the pre-edge position is related to the crystal-field splitting, which is related to the Ni-coordination (which is correlated with the average Ni-O distance). Therefore, one can estimate the average Ni-O distance with an uncertainty of ±0.01 Å in these types of oxides using this correlation between average Ni-O distance and Ni K-pre-edge position, assuming that the pre-edge position is measured with the same level of resolution and accuracy as in this study.

3.1.3. Silicate glasses

Figure 5 shows the normalized XANES spectra for Ni in a variety of silicate glasses containing from 40 ppm to 22.7 wt.% NiO, with NBO/T ratios ranging from 0 (albitic) to 1 (Na or K-disilicate). Table 3 shows the pre-edge information for these glasses (data are plotted in Fig. 6). For the sodic glasses, there is little influence of either NBO/T ratio or Ni-content on the average Ni-coordination, which remains constant near 5.0 (average Ni-O distance, ⟨Ni-O⟩ = 2.00 ± 0.02 Å). The pre-edges for the two calcic glasses are located on the high energy side of the domain for $^{[5]}$Ni, resulting in slightly higher predicted ⟨Ni-O⟩ ~ 2.02–2.03(1) Å. In contrast, the pre-edge information for potassic glasses is consistent with the presence of dominantly $^{[4]}$Ni (⟨Ni-O⟩ ~ 1.95(1) Å).

The XANES spectra for all glasses (Fig. 5) show a white line (feature C) and a shoulder (feature D) that are similar to those in the calculated spectra for 5- or 6-coordinated Ni (see Fig. 4). However, because of the presence of a relatively intense pre-edge peak (feature A) and a moderate "white line" (feature C), the K-edge XANES spectra for Ni in the glasses studied here are more consistent with dominant amounts for 5-coordinated Ni. No additional features in the Ni K-edge XANES of the glasses were observed. Such additional features, if present, could indicate minor levels of 4- and 6-coordinated Ni or/and the presence of next-nearest neighbors around Ni (network formers and modifiers) and/or multiple scattering features (high probability, based on theoretical calculations using FEFF) or/and multi-electronic excitations (low probability but an accurate estimation is required).

3.2. EXAFS

3.2.1. Model compounds

Figure 7 shows the raw, normalized, and k^3-weighted EXAFS spectra for selected Ni-model compounds. Their corresponding FTs are shown in Figure 8. The first peak in the FTs near 1.6 Å (FTs are uncorrected for Ni-O phase-shifts) corresponds to the Ni-O correlation pair. The medium-range environment around Ni (peaks above 3 Å on the FT; Fig. 8) in the model compounds examined is variable, ranging from highly ordered in NiO to relatively disordered in Ni-bearing olivine (α-Ni : Mg_2SiO_4, with two octahedral sites, M1 and M2, and preferential partitioning of Ni into the M1 site). Table 4 shows the EXAFS-derived structural parameters obtained for the oxygen environment around Ni in these model compounds. The EXAFS-derived mean ⟨Ni-O⟩ distances are, on average, within 0.02 Å of the values obtained from X-ray diffraction. The EXAFS-derived coordination numbers are within 20% of the X-ray diffraction-derived coordination numbers. The results of fitting by using both the cumulant expansion and analytical distribution function treatments of anharmonicity are very similar (except for the $\Delta\sigma^2$ values, which may vary depending on the model used). The anharmonic parameter (ΔC_3) is not negligible in $K^{[5]}NiPO_4$, suggesting that disorder effects are important in some of these materials. However, because the average Ni-O distance is within 0.02 Å of that expected from

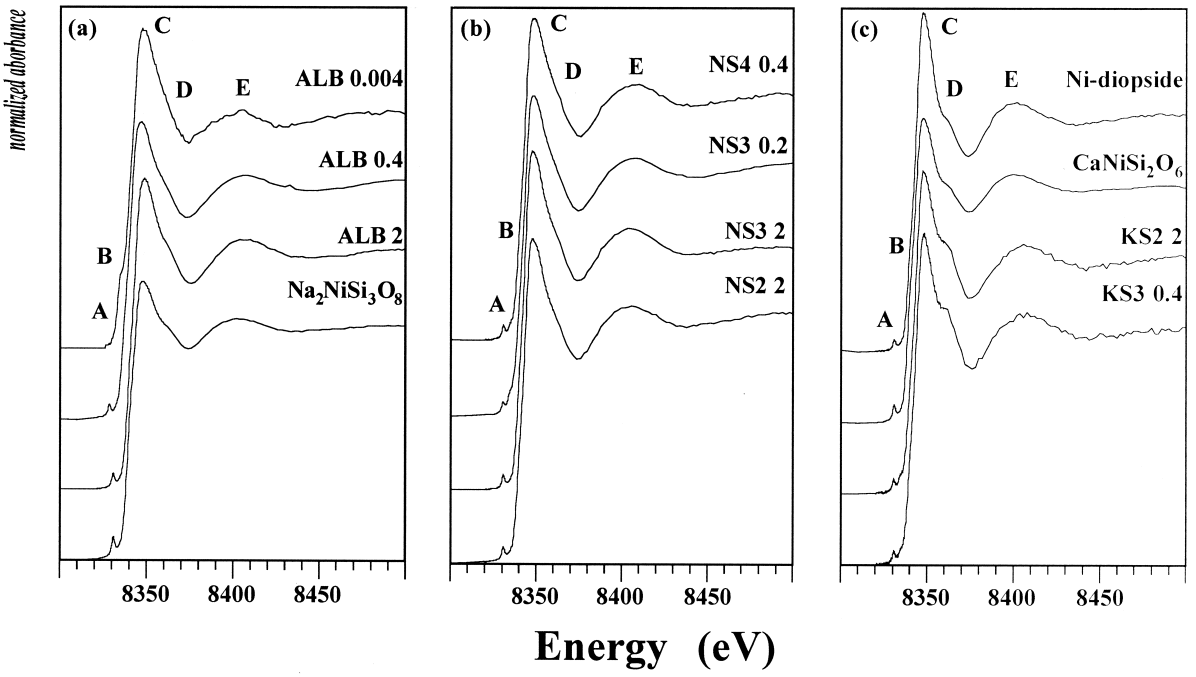

Fig. 5. Ni K-edge XANES spectra for the glasses of this study. (a, left) albitic glasses; (b, middle) other sodic glasses; (c, right) calcic and potassic glasses. A is the pre-edge feature, C the edge crest, and D the first EXAFS oscillation.

X-ray diffraction measurements, this anharmonic model (cumulant expansions theory) appear to work well, even for highly disordered oxygen environments around Ni.

In Ni-bearing olivine and diopside, EXAFS results are consistent with pre-edge information, and suggest the presence of distorted 6-coordinated environments in these phases, as expected. There are major differences in the medium-range environment of Ni in the Ni-bearing silicates relative to their respective Ni-rich end-members, α-Ni_2SiO_4 or $CaNiSi_2O_6$ (see Fig. 8). These differences may be due to different second- and third-neighbor environments around Ni when it substitutes in small amounts for Mg in olivines (Galoisy et al., 1995) and clinopyroxenes.

Table 3. Ni pre K-edge information for the Ni-bearing silicate glasses.

	Pre-edge information		
Glass	Normalized height	Absolute position (eV)	Half-width (eV)
KS2 2	0.045	8330.80	1.54
KS3 0.4	0.045	8330.78	1.49
NS2 2	0.038	8331.03	1.58
NS2 0.4	0.038	8330.99	1.59
NS2 0.004	0.037	8331.06	1.55
NS3 2	0.040	8330.98	1.52
NS3 0.4	0.038	8330.96	1.57
NS4 0.4	0.035	8330.91	1.45
$Na_2NiSi_3O_8$	0.038	8330.00	1.54
ALB 2	0.041	8330.89	1.50
ALB 0.4	0.037	8331.05	1.60
ALB 0.4 at 1150°C	0.035	8331.02	1.50
$CaNiSi_2O_6$	0.036	8331.08	1.58
Ni : $CaMgSi_2O_6$	0.036	8331.08	1.58
Average error	0.002	0.05	0.05

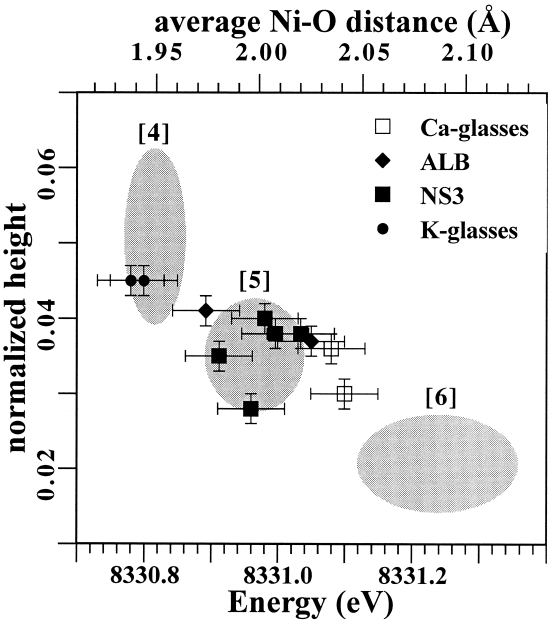

Fig. 6. Plot of pre-edge information for the glasses of this study superimposed on the template from Fig. 3b, which is based on model compounds. Sodium silicate glasses are located in the domain corresponding to an average coordination of Ni ~ 5.0.

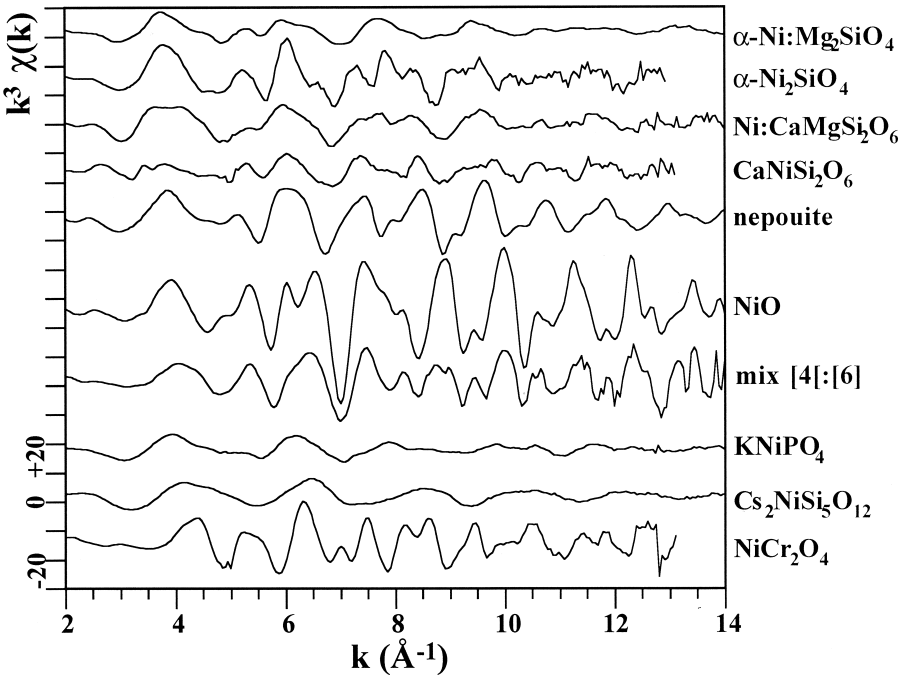

Fig. 7. Ni K-edge normalized, k^3-weighted EXAFS spectra for model compounds of this study.

3.2.2. Silicate glasses

Figure 9a shows the raw, normalized, k^3-weighted EXAFS spectra for selected silicate glasses (see Galoisy and Calas, 1993a for EXAFS spectra of potassium bearing glasses) and their corresponding best models calculated, assuming O and Si first-, and second neighbors (see below). Figure 9b show the FTs for the experimental spectra shown on Figure 9a. For all glasses, a Ni-O peak is observed near 1.5 Å in the FTs. Table 5 shows the anharmonic, least-squares-fitting results obtained from the models presented in Figure 9a. The fit-quality parameter ΔE_0 is within the experimental resolution. The EXAFS-derived average Ni-O distance is 1.97 to 2.03 Å for the glasses considered. The EXAFS-derived distances are in good agreement with those estimated from the pre-edge position (see

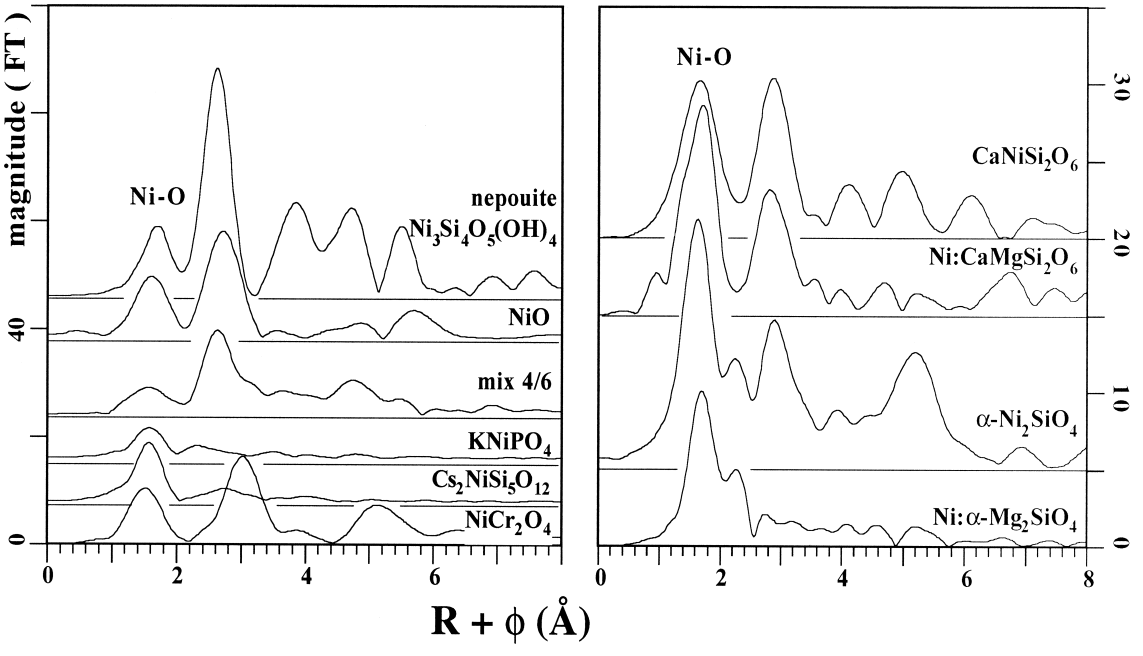

Fig. 8. Fourier Transforms of the normalized, k^3-weighted EXAFS spectra for model compound EXAFS spectra shown in Fig. 7.

Table 4. EXAFS least-squares fitting results for the Ni-O pair correlation in selected model compounds compared to X-ray diffraction-derived Ni-O distances, where available (in bold).

	Structural data[a]				Fit quality	
	N	⟨R⟩ (Å)	$\Delta\sigma^2$ (Å^2)	ΔC_3 (Å^3)	ΔE_0 (eV)	$\chi^{2\,b} \times 10^2$
$^{[4]}NiCr_2O_4$						
4 × O at 1.95 Å	4.2 (1)	1.96 (1)	0.523 (3)	0.000 (1)	−1.2 (4)	0.77
$Cs_2{}^{[4]}NiSi_5O_{12}$						
4 × O at 1.88 Å	4.4 (2)	1.92 (1)	0.332 (5)	0.000 (0)	−2.3 (8)	3.30
$K^{[5]}NiPO_4$						
5 × O at 2.01 Å	5.0 (1)	2.02 (1)	4.321 (2)	0.003 (1)	−1.3 (7)	0.021
50 : 50 mix 4 : 6 (2 × O at 1.95 Å and 3 × O at 2.08 Å)						
5 × O at 2.03 Å	5.7 (2)	2.04 (1)	2.243 (1)	0.001 (1)	−2.0 (11)	0.427
$^{[6]}NiO$						
6 × O at 2.08 Å	5.6 (1)	2.08 (1)	0.048 (5)	0.000 (1)	−2.1 (9)	0.606
$^{[6]}Ni_3Si_2O_5(OH)_3$						
6 × O at 2.07 Å	5.9 (2)	2.06 (1)	0.321 (4)	0.000 (1)	−0.0 (2)	0.014
α-$^{[6]}Ni_2SiO_4$						
6 × O at 2.09 Å	5.8 (2)	2.09 (1)	5.740 (8)	0.001 (1)	+1.4 (2)	0.359
$Ca^{[6]}NiSi_2O_6$						
6 × O at 2.08 Å	5.5 (2)	2.09 (1)	2.655 (3)	0.001 (1)	+1.5 (5)	6.716
$^{[6]}Ni$: α-Mg_2SiO_4						
	5.5 (3)	2.09 (2)	4.390 (5)	0.000 (0)	−0.7 (2)	0.024
$CaMg_{0.9}{}^{[6]}Ni_{0.1}Si_2O_6$						
	6.1 (3)	2.08 (2)	4.100 (6)	0.000 (1)	+1.2 (4)	1.010

[a] Absolute values, calculated by using FEFF8 ab initio amplitude and phase functions.
[b] χ^2 of the least-squares fit to the data.
N, ⟨R⟩, $\Delta\sigma^2$, and ΔC_3 are the total number of O first neighbors around Ni (±20%), the average Ni-O distance (±0.01 Å), the relative Debye–Waller type-factor (±0.005 Å^2), and the relative third cumulant (±0.001 Å^3), and the asymmetry parameter (±0.1), respectively.

earlier discussion in Section 3.1.3). The average Ni-O distance is slightly shorter for the albitic glasses (1.97–1.98 Å) and slightly longer for the calcic glasses (2.02–2.03 Å) than the average value for 5-coordinated Ni(II), again in agreement with the distances estimated from the pre-edge positions (and Ni-O distances derived from neutron scattering for the $CaNiSi_2O_6$ glass; Gaskell et al., 1992; see also Galoisy and Calas, 1991). The anharmonic parameter, ΔC_3, although small, is not negligible, indicating a small amount of positional disorder in the first- and second-coordination shells around Ni in these glasses.

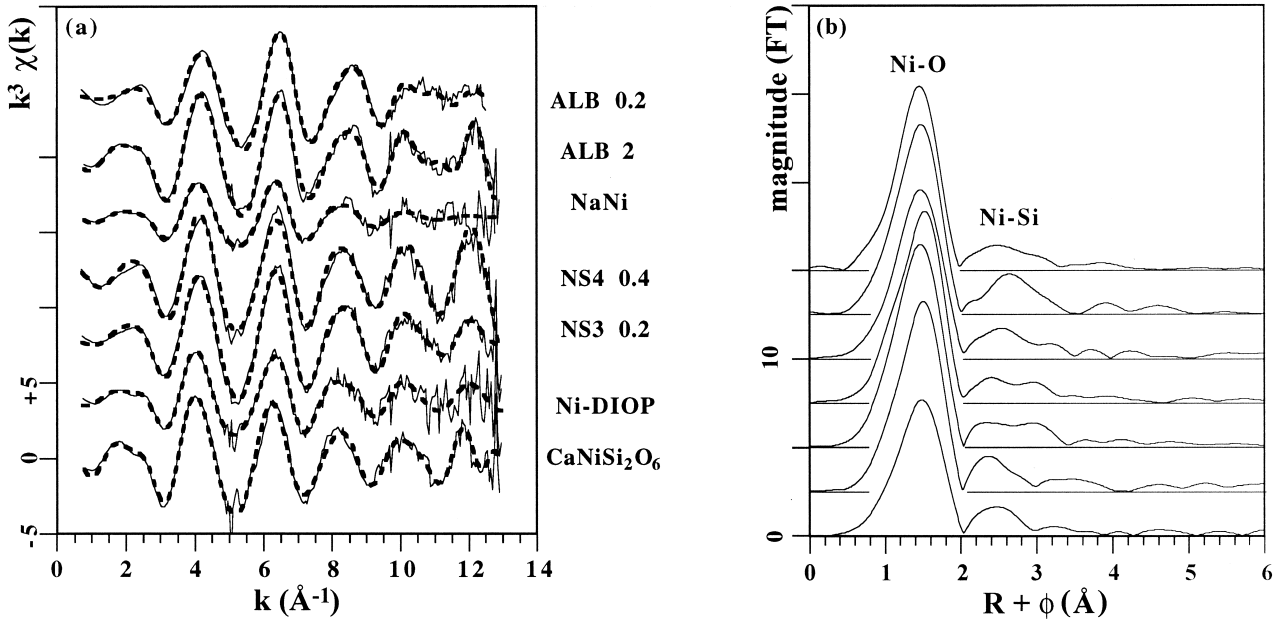

Fig. 9. (a, left) Ni K-edge normalized, k^3-weighted EXAFS spectra for selected glasses and the best model fit to these spectra assuming two shells of O and Si neighbors around Ni; (b, right) FTs of the spectra shown in on Fig. 9a.

Table 5. EXAFS least-squares fitting results for the Ni-O and Ni-Si pair correlations in selected Ni-bearing silicate glasses (calculated errors are in parentheses).

		Structural data[a]				Fit quality		
	Shell	N	⟨R⟩ (Å)	$\Delta\sigma^2$ (Å^2)	ΔC_3 (Å^3)	E_0 (eV)	ΔE_0 (eV)	$\chi^{2\,b} \times 10^2$
Ni : $CaMgSi_2O_6$	O	5.2 (8)	2.02 (1)	0.2 (1)	0.4 (1)	8339.5 (4)	−1.0	0.196
	Si	3 (1)	3.19 (3)	0.2 (1)	2.4 (2)		−4.0	
$CaNiSi_2O_6$	O	5.2 (5)	2.03 (1)	0.3 (1)	1.1 (1)	8339.5 (1)	−1.0	0.283
	Si	2 (1)	3.19 (3)	0.3 (1)	0.0 (1)		−1.1	
NS4 0.4	O	5.3 (4)	1.99 (1)	0.1 (1)	0.3 (2)	8339.4 (4)	0.9	0.751
	Si	2 (1)	3.18 (5)	0.4 (1)	0.0 (2)		0.1	
NS3 0.2	O	4.7 (6)	1.99 (1)	0.2 (1)	0.5 (3)	8337.8 (4)	0.0	0.588
	Si	2 (1)	3.28 (3)	0.7 (2)	0.0 (1)			
$Na_2NiSi_3O_8$	O	5.3 (5)	1.98 (1)	0.2 (1)	0.2 (1)	8339.1 (2)	0.3	0.623
	Si	3 (1)	3.19 (3)	2.0 (1)	1.0 (1)		0.8	
ALB 2	O	4.6 (5)	1.97 (1)	0.2 (1)	0.1 (1)	8338.1 (2)	−1.4	0.645
	Si	3 (1)	3.27 (3)	0.6 (1)	0.5 (1)		5.6	
ALB 0.4	O	4.6 (6)	1.98 (1)	0.2 (1)	1.2 (2)	8338.0 (4)	−0.9	0.985
	Si	3 (1)	3.25 (4)	0.4 (2)	0.0 (0)		−1.7	
Average least-squares precision	O	0.5	0.01	0.1	0.1	0.5	0.5	
	Si	1	0.05	0.2	0.2		0.5	

[a] Absolute values, calculated by using FEFF8 ab initio amplitude and phase functions.
[b] χ^2 of the least-squares fit to the data.
N, ⟨R⟩, $\Delta\sigma^2$, and ΔC_3 are the total number of O first neighbors around Ni (±20%), the average Ni-O distance (±0.01 Å), the relative Debye–Waller type-factor (±0.005 Å^3), and the relative third cumulant (±0.001 Å^3), respectively.

Another contribution to the EXAFS is observed near 2.9 Å in the FTs. Ab initio calculations, using the FEFF8 code based on the structure of $Cs_2{}^{[4]}NiSi_5O_{12}$ and $K^{[5]}NiPO_4$, suggest that multiple scattering within the NiO_4 and NiO_5 coordination spheres does not contribute significantly to the FT feature near 3 Å observed for some of the glasses. This small contribution is best fit by Si atoms in the medium-range environment around Ni in these glasses. The average Ni-Si distance is 3.20(5) Å, and the number of Si second neighbors is relatively small (2 ± 1 Si). Here again, the anharmonic parameters are relatively small. As for previous EXAFS studies (Galoisy and Calas, 1993a, b), there is no clear evidence for Ni-Ni pairs, as detected by neutron-scattering on concentrated Ni-glasses, like $CaNiSi_2O_6$ (Cormier et al., 1995). This is related to the large structural disorder in the medium-range environment of Ni in silicate glasses, which strongly limits the possible paths of the photoelectron induced by synchrotron X-rays.

4. DISCUSSION

4.1. Coordination of Ni in Silicate Glasses and Melts

Our new XAFS data analysis protocols for Ni(II) in silicate glasses involving high-resolution pre-edges, XANES analysis, and explicit treatment of anharmonic effects provide a coherent picture of the local coordination environment of Ni in the silicate glasses examined here. By accurately monitoring the pre-edge position, we are able to derive an average coordination for Ni of ~5.0 oxygens for all sodic and ~5.3 oxygens for the calcic silicate glasses investigated. The estimated average Ni-O distances based on the pre-edge position for these glasses are 1.97 to 2.04 Å (Fig. 6), which are consistent with the EXAFS-derived distances (1.97–2.03 Å; Table 5). The results of this anharmonic data analysis protocol are generally consistent with those from previous studies on more concentrated glasses derived by using the standard harmonic EXAFS model (Galoisy and Calas, 1993a), although the average Ni-O distances are slightly higher in our analysis, which is consistent with slightly higher average coordination of Ni.

The effect of Ni concentration (which ranges from 2 wt.% to 40 ppm for albite glass) on the local environment of Ni in our silicate glasses is quite small. These results are consistent with solubility measurements of Ni in silicate melts of various compositions (Dingwell et al., 1994; Ertel et al., 1997; Fortenfant and Dingwell, 1998), which suggest that the minimum in Ni solubility (~1800 ppm) is found for compositions poor in alkalis (<25 mol.% Na or K-metasilicate in haplobasaltic and anorthite-diopside eutectic melt compositions). Although the EXAFS spectrum for the most dilute glass (ALB 0.004) cannot be analyzed even though we collected and averaged a number of scans, its Ni K-edge XANES spectrum (Fig. 5a) is similar to those of the other ALB glasses examined in this study. Finally, we have investigated the effect of NBO/T in sodic glasses and found that there is no detectable effect within the EXAFS least-squares fitting errors.

The pre-edge analysis protocol is not able to establish directly if the sodic glasses contain mostly 5-coordinated Ni or a ~50 : 50 mixture of $^{[4]}$Ni and $^{[6]}$Ni. However, the disorder parameters ($\Delta\sigma^2$) for the sodic glasses are much smaller (<0.01 Å^2) than that measured for the 50 : 50 mixture of $^{[4]}$Ni and $^{[6]}$Ni (~0.022 Å^2; Table 4). Therefore, we conclude that Ni is present dominantly in one coordination environment in sodic glasses, possibly as trigonal bipyramids, based on previous crystal-field spectroscopy interpretations (Galoisy and Calas, 1993a). Indeed, this geometry is the dominant one around $^{[5]}$Ni in Ni-containing oxide-type compounds (see Nord and Stefanidis, 1981 for a short review). Thus, the pre-edge positions, intensities of the pre-edge features, and EXAFS parameters are not consistent with dominant amounts of NiO_6 sites in any of

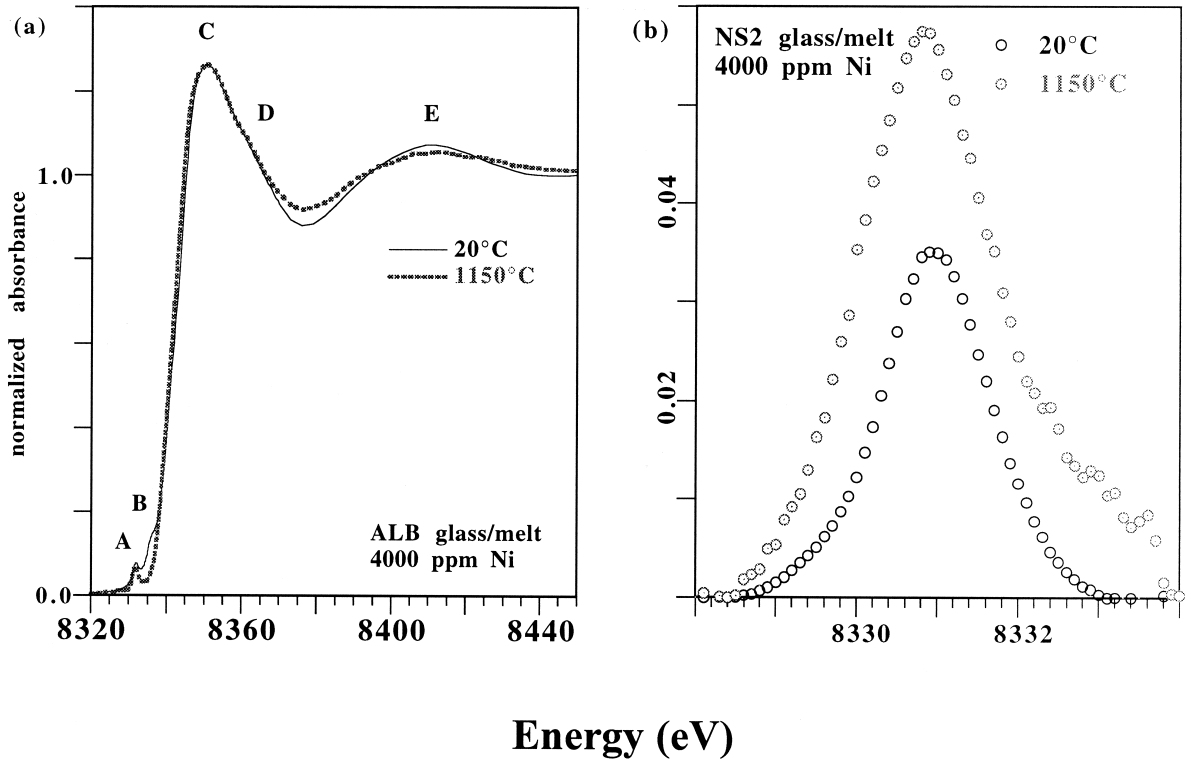

Fig. 10. (a, left) Ni K-edge XANES spectra (ID 26, ESRF) collected from an albitic glass and melt to 1150°C containing 4000 ppm Ni; (b, right) normalized pre-edges (feature A in Fig. 10a), showing an enhanced contribution due to tetrahedral Ni(II) in the melt phase of sodium-disilicate.

these glasses. However, a continuous range of sites for Ni, ranging from 4- to 6-coordinated Ni environments, is likely to be present in all the glasses investigated, as indirectly suggested by crystal-field spectroscopy of Ni (see Galoisy and Calas, 1993a) and molecular dynamics of the isostructural Fe(II) in a silicate glass of hedenbergite composition (Rossano et al., 2000). For instance, the quench rates for sodic glasses influence highly the color of these glasses, ranging from deep brownish-violet (for very fast quench rates) to brownish (relatively slower quench rates), suggesting the presence of lower coordination environments around Ni in ultra-quenched glasses.

Our finding of dominantly 5-coordinated Ni in the sodic silicate glasses examined here is in contrast with the coordination of Ni in sodic melts. Ni K-edge XANES and EXAFS information reported for a sodium disilicate melt containing 2 wt.% of Ni (Farges et al., 1994) suggested the presence of dominant amounts of 4-coordinated Ni. This result is confirmed in this study for lower Ni-concentrations and more polymerized compositions (Fig. 10a,b). In situ, Ni K-edge XANES and pre-edge information for Na-disilicate and albitic melts, both doped with 4000 ppm Ni, were collected by using a newly designed undulator spectrometer (ID26 at ESRF, Grenoble), now available on third generation synchrotron sources. The Ni pre-edge spectrum for both melts (1150°C and 1350°C, respectively) is typical of 4-coordinated Ni(II) and is shifted by 0.15 eV toward lower energy and increased two times in normalized height as compared to the room temperature glass spectrum, in excellent agreement with crystal-field interpretations of an albitic sample doped with 2 wt.% Ni (Keppler, 1996).

4.2. Medium-Range Environments of Ni in Silicate Glasses

Our EXAFS analysis detects a contribution near 3 Å in the FTs (uncorrected for phase shift) for most of the glasses examined which is not caused by multiple scattering (based on ab initio EXAFS calculations for the $KNiPO_4$ model compound). Instead, the presence of second-neighbor Si atoms (based on EXAFS fitting results, see Section 3.2.2) is the most likely cause of this feature. The presence of Si atoms at 3.2 Å (Ni-O-Si angle ~125°, assuming a Si-O distance of ~1.6 Å in silicate glasses; Brown et al., 1995) from the central Ni atoms is similar to the medium-range structure around Ni in crystalline $Cs_2NiSi_5O_{12}$ (except that the Ni-coordination is 4 in that model compound). In this leucite-related structure, NiO_4 and SiO_4 tetrahedra share corners with average inter-tetrahedral Ni-O-Si angles (135°) that are lower than the mean Si-O-Si angles (144°), in agreement with the inverse correlation between T-O bond length and the mean T-O-T angle in framework silicates (Brown et al., 1969; Hill and Gibbs, 1979; Navrotsky et al., 1985). Because of the similarities in the XANES and EXAFS spectra between Ni-bearing leucite and silicate glasses, alkalis should also be present around Ni, but at distances above 3.5 Å, and with a range of distances, which makes them difficult to detect with EXAFS and XANES methods. Indeed, the bonding of NiO_n polyhedra ($n = 4, 5, 6$) to network modifiers is strongly suggested by: 1) the variation of average Ni-coordination in the Ni-silicate glasses examined with different network modifiers (Na, K, and Ca); 2) the Ni

solubility data (which is low in alkali-poor compositions; Fortenfant and Dingwell, 1998) and bond valence models (Galoisy and Calas, 1993a,b).

Then, generic bond-valence models for Ni in the silicate glasses investigated here can be depicted as follows in potassic, sodic, and calcic glasses:

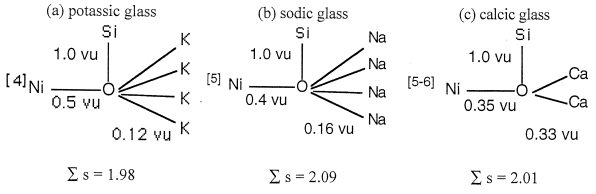

By applying Pauling's second rule to these three examples, one can extract an unified Pauling relationship:

$$\sum_{\text{cations}} s = s_{Ni} + \sum_{NF} s_{NF} + \frac{Z_{NF}}{Z_{NM}} \times \sum_{NM} s_{NM} \qquad (1)$$

in which s_{Ni}, s_{NF}, and s_{NM} as the average bond valence for the Ni-O, NF (network-former)-O and NM (network-modifier)-O bonds. Z_{NF} and Z_{NM} hold for the formal valence of network formers to network modifiers, respectively.

Because of Pauling's second rule, one can also write:

$$s_{Ni} = \frac{2}{N_{Ni}} \quad \text{and} \quad \sum_{\text{cations}} s = |Z_O| \qquad (2,3)$$

from which, we can extract N_{Ni}, the predicted nickel coordination:

$$N = \frac{2}{2 - \frac{Z_{NF}}{Z_{NM}} + s_{NM} - s_{NF}} \qquad (4)$$

These predictions are only estimates as we have postulated average Pauling bond valences of 0.12 (= 1/8), 0.16 (= 1/6), and 0.33 (= 1/6) for K, Na, and Ca in silicate glasses (see Brown et al., 1995). Also, more distant charge compensation effects are not taken into account. However, one can reproduce the trends observed experimentally with this simple approach. The predicted nickel coordination numbers (CN) for sodic, potassic, and calcic glasses using this model (3.9, 5.5 and 5.9) matches the experimental data (4.0, 5.0, and 5.3) at ±0.5 CN units. Also, melts are characterized by lower average bond valences (−0.04 valence units at 1500 K around Na; see Brown et al., 1995), which result from the relatively higher thermal expansion of weakly-bonded network modifiers. By using Eqn. 4, the calculated average Ni-coordination number (3.8) for Ni in sodic melts is in excellent agreement with the XANES and EXAFS information reported for a sodium disilicate melt containing 2 wt.% of Ni (Farges et al., 1994) and also with the XANES and pre-edge information for a molten albite doped with 4000 ppm Ni (Fig. 10).

4.3. Conclusions and Prospectives for High-Pressure Hydrous Glasses and Melts

Ni-bearing melts are characterized by lower average Ni coordination numbers, which is related to the relatively higher thermal expansion of network modifiers to which Ni adapts its continuum of possible sites (Brown et al., 1995). The coordination environment of transition metal ions in silicate glasses and melts is controlled by several factors. First, the relative flexibility of individual metal-oxygen first-neighbor bond distances (particularly around network modifiers such as Na and Ca) makes that these cations can adapt for a given bonding situation as a function of pressure, temperature or composition. This effect is related to the relative difficulty to define a coordination number *sensu-stricto* for such cations in disordered systems, so the variety of local topologies existing in glasses and melts is adequate for transition elements. This is generating a continuum of environments, centered to the value measured by XAFS spectroscopy. Second, the general requirement of Pauling's bond valence sum rule should be satisfied in silicate glasses and melts (Farges et al., 1991; Galoisy and Calas, 1993a; Brown et al., 1995).

Based on these type of structural models, a "complexation" of Ni by OH^- groups or water molecules should result in dramatic changes in the local structural environment of Ni, because protons in the form of hydroxyl groups contribute ~0.7 valence units to the bond valence sum, which is three times higher than the amount contributed by alkalis. Part II of this series focuses on the effect of water on the local environment of Ni in sodium silicate melts quenched from 5 kbars where changes in the local structural environment around Ni are dramatic.

Acknowledgments—The authors want to particularly thank Laurence Galoisy and Isabelle Martinez (both at Université de Paris 7) for fruitful discussions and for providing the α-Ni_2SiO_4 and Ni-olivine model compounds, respectively, and C. M. B. Henderson (University of Manchester) for donating the $Cs_2NiSi_5O_{15}$ leucite sample and for reviewing accurately this manuscript. This work was supported by the EEC TMR network "Water in Molten Silicates" (FF) and by National Science Foundation Grant EAR-9725899 (G.E.B.). The Stanford Synchrotron Radiation Laboratory is supported by the U.S. Department of Energy, Office of Basic Energy Sciences and Office of Biological and Environmental Research, and the U.S. National Institutes of Health, Biotechnology Resource Program, Division of Research Resources. The work done at the ESRF was supported by the ESRF (proposal # CH-768).

Associate editor: D. B. Dingwell

REFERENCES

Ankudinov A. L., Ravel B., Rehr J. J., and Conradson S. D. (1998) Real-space multiple-scattering calculation and interpretation of x-ray absorption near-edge structure. *Phys. Rev. B* **58,** 7565–7576.

Bell A. M. T. and Henderson C. M. B. (1996) Rietveld refinement of the orthorhombic Pbca structures of $Rb_2CdSi_5O_{12}$, $Cs_2MnSiO_5O_{12}$, $Cs_2CoSi_5O_{12}$ and $Cs_2NiSi_5O_{12}$ leucites by synchrotron X-ray powder diffraction. *Acta Crystallogr. C* **52,** 2132–2139.

Brindley G. W. and Wan H. M. (1975) Compositions, structures and thermal behavior of nickel-containing minerals in the lizardite-nepouite series. *Am. Mineral.* **60,** 863–871.

Bobrovskii A. B., Kartmazov N., and Finkel V. A. (1973) (no title) *Izv. Akad. Nauk. SSSR* (Neorganic Materials) **9,** 1075–1076.

Brown F. C. (1980) Inner-shell threshold spectra. In *Synchrotron*

Radiation Research (eds. H. Winick and S. Doniach), pp. 61–100. Plenum Press.

Brown G. E., Jr., Gibbs G. V., and Ribbe P. H. (1969) The nature and variation in length of the Si-O and Al-O bonds in framework silicates. *Am. Mineral.* **54,** 1044–1061.

Brown G. E., Jr., Farges F., and Calas G. (1995) X-ray scattering and x-ray spectroscopy studies of silicate melts. In *Structure, Dynamics, and Properties of Silicate Melts. Reviews in Mineralogy* (eds. J. F. Stebbins, D. B. Dingwell, and P. F. McMillan), Vol. 32, pp. 317–410. The Mineralogical Society of America.

Burns R. G. (1993) *Mineralogical Applications of Crystal Field Theory*, 2nd Ed. Cambridge University Press.

Calas G. and Petiau J. (1983) Structure of oxide glasses. Spectroscopic studies of local order and crystallochemistry. Geochemical implications. *Bull. Minéral.* **106,** 33–55.

Colson R. O., McKay G. A., and Taylor L. A. (1988) Temperature and composition dependencies of trace element partitioning; olivine/melt and low-Ca pyroxene/melt. *Geochim. Cosmochim. Acta* **52,** 539–553.

Cormier L., Creux S., Galoisy L., Calas G., and Gaskell P. (1995) Medium range order around cations in silicate glasses. *Chem. Geol.* **128,** 77–91.

Courtial P., Dingwell D. B., Gottsmann J., and Holzheid A. (1997) The influence of nickel on the density of silicate melts (AGU 1997 Fall Meeting, Washington, DC). EOS, Transactions, **79**(Suppl.), 374 (abstract).

Crozier E. D., Rehr J. J., and Ingalls R. (1988) Amorphous and liquid systems. In *X-ray Absorption. Principles, Applications, Techniques of EXAFS, SEXAFS and XANES. Chemical Analysis.* (eds. D. C. Koningsberger and R. Prins), Vol. 92, pp. 373–442. John Wiley & Sons.

Dingwell D. B., O'Neill H. St. C., Ertel W., and Spettel B. (1994) The solubility and oxidation of nickel in silicate melt at low oxygen fugacities; results using a mechanically assisted equilibration technique. *Geochim. Cosmochim. Acta* **58,** 1967–1974.

Ertel W., Dingwell D. B., and O'Neill H. St. C. (1997) Compositional dependence of the activity of nickel in silicate melts. *Geochim. Cosmochim. Acta* **61,** 4707–4721.

Farges F. and Brown G. E. Jr. (1996) An empirical model for the anharmonic analysis of high-temperature XAFS spectra of oxide compounds with applications to the coordination environment of Ni in NiO, γ-Ni_2SiO_4 and Ni-bearing Na-disilicate glass and melt. *Chem. Geol.* **128,** 93–106.

Farges F., Brown G. E. Jr., Calas G., Galoisy L., and Waychunas G. A. (1994) Structural transformation in Ni-bearing $Na_2Si_2O_5$ glass and melt. *Geophys. Res. Lett.* **21,** 1931–1934.

Farges F., Brown G. E. Jr., and Rehr J. J. (1996a) Coordination chemistry of Ti(IV) in silicate glasses and melts. I. XAFS study of Ti coordination in oxide model compounds. *Geochim. Cosmochim. Acta* **60,** 3023–3038.

Fortenfant S. and Dingwell D. B. (1998) Experimental study of the compositional dependence of Ni activity in silicate melts. Bayerische Geoinstitut, Annual report, 1998, § 3.6g.

Galoisy L. and Calas G. (1991) Spectroscopic evidence for five-coordinated Ni in $CaNiSi_2O_6$ glass. *Am. Mineral.* **76,** 1777–1780.

Galoisy L. and Calas G. (1993a) Structural environment of nickel in silicate glass/melt systems. I. Spectroscopic determination of coordination states. *Geochim. Cosmochim. Acta* **57,** 3613–3626.

Galoisy L. and Calas G. (1993b) Structural environment of Ni in silicate glass/melt systems: Part 2. Geochemical implications. *Geochim. Cosmochim. Acta* **57,** 627–3633.

Galoisy L., Calas G., and Brown G. E. Jr. (1995) Intracrystalline distribution of nickel in San Carlos olivine: An EXAFS study. *Am. Mineral.* **80,** 1089–1092.

Garcia J., Blasco J., Proietti M. G., and Benfatto M. (1995) Analysis of the X-ray-absorption near-edge-structure spectra of $La_{1-x}Nd_xNiO_3$ and $LaNi_{1-x}Fe_xO_3$ perovskites at the nickel K edge. *Phys. Rev. B* **52,** 15823–15828.

Gaskell P. H., Zhao J., Calas G., and Galoisy L. (1992) The structure of mixed cation oxide glasses. In *Physics of Non-Crystalline Solids VII* (eds. L. D. Pye, W. C. LaCourse, and H. V. Stevens), pp. 53–58. Taylor and Francis.

Gauthier C., Solé V. A., Signorato R., Goulon J., and Moguiline E. (1999) The ESRF beamline ID26: X-ray absorption on ultra dilute sample. *J. Synchrotron Radiat.* **6,** 164–166.

Ghose S., Wan C., and Okamura F. P. (1987) Crystal structures of $CaNiSi_2O_6$ and $CaCoSi_2O_6$ and some crystal-chemical relations in C2/c clinopyroxenes. *Am. Mineral.* **71,** 375–381.

Greaves C. and Thomas M. A. (1986) Refinement of the structure of deuterated nickel hydroxide, $Ni(OD)_2$, by powder neutron diffraction and evidence for structural disorder in samples with high surface area. *Acta Crystallogr. B* **42,** 51–55.

Holzheid A., Palme H., and Chakraborty S. (1996) The activities of NiO, CoO and FeO in silicate melts. *Chem. Geol.* **139,** 21–38.

Heumann D., Dräger G., and Bocharov S. (1997) Angular-dependance in the K pre-edge XANES of cubic crystals: the separation of the empty metal e_g and t_{2g} states of NiO and FeO. *J. Phys. IV France 7* **C2,** 481–483.

Hill R. J. and Gibbs G. V. (1979) Variation in d(T-O), d(T . . . T), and delta TOT in silica and silicate minerals, phosphates and aluminates. *Geol. Soc. Am.* (Abstr. Programs) **10,** 421.

Keppler H. (1992) Crystal field spectra and geochemistry of transition metal ions in silicate melts and glasses. *Am. Mineral.* **77,** 62–75.

Keppler H. (1996) The investigation of phase transitions by electronic absorption spectroscopy. *Phys. Chem. Minerals* **23,** 288–296.

Kinzler R. J. (1990) An experimental study on the effect of temperature and melt composition on the partitioning of nickel between olivine and silicate melt. *Geochim. Cosmochim. Acta* **54,** 1255–1265.

Kosarev E. L. (1990) Shannon's super resolution limit for signal recovery. *Inverse Problems* **6,** 55–76.

Kuzmin A., Purans J., and Rodinov A. (1997) X-ray absorption spectroscopy study of the Ni K-edge in magnetron-sputtered nickel oxide think films. *J. Phys. Condens. Matter* **9,** 6979–6993.

Lager G. A. and Meagher E. P. (1978) High-temperature structural study of six olivines. *Am. Mineral.* **63,** 365–377.

Lytle F. W., Greegor R. B., Sandstrom D. R., Marques D. R., Wong J., Spiro C. L., Huffman G. P., and Huggins F. E. (1984) Measurement of soft x-ray absorption spectra with a fluorescence ion chamber detector. *Nucl. Inst. Meth.* **226,** 542–548.

Lyutin V. I., Tutov A. G., Illyukhin V. V., and Belov V. V. (1973) Crystal structure of the antiferromagnetic K, Ni phosphate $KNiPO_4$. *Sov. Phys. Dokl.* **18,** 12–14.

Malavergne V., Guyot F., Wang J., and Martinez I. (1997) Partitioning of nickel, cobalt and manganese between silicate perovskite and periclase: A test of crystal field theory at high pressure. *Earth Planet. Sci. Lett.* **146,** 499–509.

Manceau A. and Calas G. (1986) Nickel-bearing clay minerals: 2. Intracrystalline distribution of nickel: An x-ray absorption study. *Clay Mineral.* **21,** 341–360.

Mysen B. O., Drake M. J., and Holloway J. R. (1982) Partitioning of Ni between olivine and silicate melt; the "Henry's law problem" reexamined—discussion and reply. *Geochim. Cosmochim. Acta* **46,** 297–299.

Navrotsky A., Geisinger K. L., McMillan P. F., and Gibbs G. V. (1985) The tetrahedral framework in glasses and melts—Inferences from molecular orbital calculations and implications for structure, thermodynamics, and physical properties. *Phys. Chem. Mineral.* **11,** 284–298.

Nord A. G. and Stefanidis T. (1981) Crystal chemistry of γ-$(Zn,Me)_3(PO_4)_2$ solid solutions. *Mat. Res. Bull.* **16,** 1121–1129.

Nowak M. and Keppler H. (1998) The influence of water on the environment of transition metals in silicate glasses. *Am. Mineral.* **83,** 43–51.

Pettitfer R. F. and Hermes C. (1985) Absolute energy calibration of x-ray radiation from synchrotron sources. *J. Applied Crystallogr.* **18,** 404–412.

Rehr J. J., Zabinsky Z. I., and Albers R. C. (1992) High-order multiple scattering calculations of x-ray-absorption fine structure. *Phys. Rev. Lett.* **69,** 3397–4000.

Rossano S., Ramos A., Delaye J.-M., Creux S., Filiponi A., Brouder Ch., and Calas G. (2000) EXAFS and molecular dynamics combined study of CaO-FeO-$2SiO_2$ glass. New insight into site significance in silicate glasses. *Europhys. Lett.* **49,** 597–602.

Seifert S., O'Neill H. S. C., and Brey G. (1988) The partitioning of Fe,

Ni and Co between olivine, metal, and basaltic liquid; an experimental and thermodynamic investigation, with application to the composition of the lunar core. *Geochim. Cosmochim. Acta* **52,** 603–616.

Solé A. V., Gauthier C., Goulon J., and Natoli F. (1999) Undulator QEXAFS at the ESRF beamline ID26. *J. Synchrotron Radiat.* **6,** 174–175.

Takahashi E. (1978) Partitioning of Ni^{2+}, Co^{2+}, Fe^{2+}, Mn^{2+}, and Mg^{2+} between olivine and silicate melts: Compositional dependence of partition coefficient. *Geochim. Cosmochim. Acta* **42,** 1829–1844.

Taura H., Yurimoto H., Kurita K., and Sueno S. (1998) Pressure dependence on partition coefficients for trace elements between olivine and the coexisting melts. *Phys. Chem. Mineral.* **25,** 469–484.

Waychunas G. A., Brown G. E. Jr., and Apted M. J. (1983) X-ray K-edge absorption spectra of Fe minerals and model compounds: near edge structure. *Physics Chem. Minerals* **10,** 1–9.

Westre T. E., Kennepohl P., de Witt J., Hedman B., Hodgson K. O., and Solomon E. I. (1997) A multiplet analysis of Fe K-edge 1s → 3d pre-edge features of iron complexes. *J. Am. Chem. Soc.* **119,** 6297–6314.

Winterer M. (1996) The XAFS package. Proceedings of the 9th International Conference on X-ray Absorption Fine Structure (XAFS VI, Grenoble), 144.